*Int. J. Heat Mass Transfer.* Vol. 29, No. 4, pp. 611–623, 1986
Printed in Great Britain

0017–9310/86 $3.00 + 0.00


# Buoyancy-induced flow adjacent to a horizontal surface submerged in porous medium saturated with cold water

DONG-SHIUN LIN and BENJAMIN GEBHART
Department of Mechanical Engineering and Applied Mechanics, University of Pennsylvania, Philadelphia, PA 19104, U.S.A.

(*Received* 4 *December* 1984 *and in final form* 8 *November* 1985)

**Abstract**—Transport calculations are given for laminar boundary-layer, buoyancy-induced flow adjacent to heated or cooled horizontal surfaces submerged in a porous medium saturated with cold water wherein a density extremum may arise. The results demonstrate for the first time the existence of 'inner region of normal velocity component reversal'. This is also shown to arise for all natural convection flows adjacent to horizontal surfaces. It is noted that the Prandtl number $Pr = \nu/\alpha_1$ does not appear as an additional parameter in this formulation. A temperature parameter $R$ expresses the relation between imposed temperatures $t_0$ and $t_\infty$ and the extremum temperature $t_m$. Calculations are made for both the isothermal and uniform flux surface conditions, over a wide range of $R$, including buoyancy force reversal conditions. For an isothermal surface, the transport results for $0 \leqslant R \leqslant 0.08$ and $0.288 \leqslant R \leqslant 0.5$ include buoyancy force reversal regions. The characteristics of these two subregions are found to be different. Detailed tabulations of transport parameters are included for both the isothermal and uniform flux surface conditions. These new results are compared with those resulting from the conventional Boussinesq buoyancy force approximation.

## 1. INTRODUCTION

PURE WATER at 1 atm has a density extremum at about 4°C. This is due to a balance of the competing density-controlling mechanism of hydrogen bonding and molecular thermal motion. This anomalous density behavior has far reaching effects in buoyancy-driven transport. It also complicates analysis since the second Boussinesq approximation, that the fluid density $\rho$ varies linearly with temperature, can no longer be applied.

The transport complexity will be briefly reviewed here first for the flow adjacent to a vertical surface. Consider, for example, a vertical surface at a uniform temperature $t_0 = 8°C$, in a quiescent pure water ambient $t_\infty = 2°C$. Near the surface, the fluid is less dense than the ambient and the buoyancy force is upward. However, since extremum occurs at about 4°C, the fluid in the outer portion of the thermal transport region is more dense than the ambient. Consequently, the buoyancy force then is downward. Thus, an inside buoyancy force reversal occurs across the thermal diffusion region. An inside flow reversal may result. That is, inner flow may be up, with the outer flow down. With changing values of $t_0$ and $t_\infty$, inversion may arise. That is, the direction of net mass flow may reverse.

In the past, a very compact relation for density–temperature dependence in cold water was not available. A recent equation given in ref. [1] contains 35 temperature terms; another recent and vastly simpler equation [2] is of comparable accuracy. The latter expression contains only one temperature term. This simplicity of the temperature dependence leads to similarity solutions of boundary-layer flows.

There are many recent studies of buoyancy-driven motion in cold water, using this new density equation. Transport from isothermal and constant heat flux horizontal surfaces was calculated in ref. [3]. Qureshi and Gebhart [4] computed similarity solutions for the flow adjacent to a vertical, uniform heat flux surface in ambient water at $t_m$. Carey *et al.* [5] considered buoyancy-induced flow adjacent to a vertical, isothermal surface in pure water ambient. Mollendorf *et al.* [6] treated axisymmetric and plane plume flow in water at $t_m$. The perturbation analysis of Gebhart *et al.* [7] extended the results of refs. [4] and [6] to ambient water temperatures not equal to $t_m$. El-Henawy *et al.* [8] found multiple steady-state solutions for vertical, buoyancy-induced flow conditions in cold, pure water.

In recent years, there has been a growing interest in buoyancy-induced flow in fluid-saturated, porous media due to concerns about geothermal deposits, energy storage and insulation. Analysis is simpler than that for Newtonian fluid transport and the permissible number of boundary conditions is less. Formulation usually, therefore, allows slip at bounding surfaces, where a no-slip condition is taken for Newtonian fluids.

There has been considerable analysis and experiment concerning buoyant transport in porous media. Cheng and his co-workers [9–11] determined a series of similarity solutions. In this analysis, the Boussinesq approximation, that the fluid density $\rho$ varies linearly with temperature, was invoked. Sun *et al.* [12] applied linear stability analysis using a cubic polynomial density–temperature relationship. Yen [13] measured the effect of a density inversion on free convective heat transfer in a porous layer heated from below. Ramilison and Gebhart [14] examined the possible similarity solutions for vertical, buoyancy-induced flow in a

## NOMENCLATURE

$a, b, c, d$ defined in equations (9), (11), (12), (13), respectively
$b_x, c_x, d_x$ denotes differentiation with respect to $x$
$B$ buoyancy force, $g(\rho_\infty - \rho)$
$B_n$ normal component of buoyancy force
$c_p$ specific heat
$f$ similarity streamfunction variable defined in equation (12)
$f$ denotes fluid in equation (3)
$G$ modified Grashof number, $5(Gr_x/5)^{1/5}$
$Gr$ Grashof number
$g$ acceleration of gravity
$I_w$ total buoyancy force, equation (26)
$K$ permeability of porous medium
$k$ effective thermal conductivity of saturated porous medium
$k_s$ thermal conductivity of solid
$k_f$ thermal conductivity of fluid
$\dot{m}$ mass flow per unit width of surface
$M$ local momentum flux
$N$ constant in $d(x) = Nx^n$
$p$ pressure
$p_h$ hydrostatic pressure
$p_m$ motion pressure
$p_\infty$ ambient pressure
$P$ non-dimensional pressure, equation (13)
$Pr$ Prandtl number
$Q$ total local convected energy
$q$ exponent in density equation (4)
$R$ parameter defined in equation (10)
$Ra_x$ local Rayleigh number, equation (21)
$s$ salinity
$t$ temperature
$t_m$ temperature at which maximum density occurs for a given salinity and pressure
$t_0$ surface temperature
$t_\infty$ ambient temperature
$u$ Darcy velocity in $x$-direction
$v$ Darcy velocity in $y$-direction
$\mathbf{v}$ vector velocity
$W$ local buoyancy force defined in equation (8)
$x$ coordinate parallel to the surface
$y$ coordinate vertical to the surface.

Greek symbols
$\alpha$ coefficient in the density equation (4)
$\alpha_1$ thermal diffusivity ratio of matrix conductivity to fluid heat capacity
$\beta$ coefficient of thermal expansion
$\delta$ boundary-layer thickness
$\eta$ non-dimensional distance in boundary region
$\eta_c$ the position of $\eta$ where vertical component velocity changes from outward to inward
$\eta_\infty$ value of $\eta$ at the edge of boundary region
$\mu$ dynamic viscosity
$\nu$ kinematic viscosity
$\rho$ density
$\rho_m$ maximum density
$\rho_\infty$ density of ambient fluid
$\rho_r$ reference quantity of density
$\phi$ normalized temperature, $(t_m - t_\infty)/(t_0 - t_\infty)$
$\psi$ streamfunction
$\varepsilon$ porosity.

Superscript
$'$ denotes differentiation with respect to $\eta$.

porous medium saturated with cold water both for $d(x) = t_0 - t_\infty$ in power law or exponential relation with respect to $x$. More recently, Gebhart *et al.* [15] obtained multiple steady-state solutions for the same kind of transient using two different numerical codes, i.e. COLSYS and BOUNDS.

This study analyzes developing buoyancy-induced transport adjacent to an extensive heated or cooled horizontal surface embedded in a porous medium saturated with cold water (see Fig. 1). There is no buoyancy force component in the principal flow direction. The flow is instead driven indirectly by a buoyancy-generated pressure field. For $B = B_n$ away from the surface, low pressure, with respect to $p_\infty$, arises in the temperature region next to the surface. If negative pressure levels arise they will result in a negative pressure gradient in the increasing $x$-direction. A developing flow will thus be induced downstream. This is an 'indirect drive', since buoyancy indirectly drives

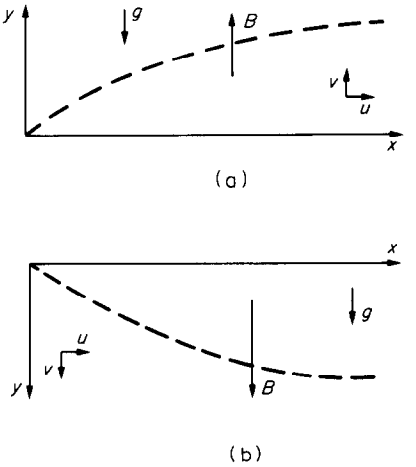


FIG. 1. Coordinate systems for the two transport conditions, buoyancy $B$ upward and downward. (a) Buoyancy effect largely upward; (b) buoyancy effect largely downward.

the flow. It produces a pressure field which, in turn, drives a relatively weak flow. Further downstream, thermal instability eventually arises, due to unstable stratification. Longitudinal vortices then may arise to separate the flow. Such a mechanism is discussed by Pera and Gebhart [16].

The following conventional assumptions simplify the analysis:

1. Flow is sufficiently slow that the convecting fluid and the porous matrix are in local thermodynamic equilibrium.
2. The physical properties of the fluid and porous matrix are uniform and isotropic.
3. Fluid remains in a single phase.
4. It is a fully saturated porous medium.
5. Darcy's law is valid.
6. Density is assumed constant except in the buoyancy force term.
7. Dufor and Sorét effects are negligible.

The density state equation used here is very accurate for both pure and saline water to a pressure level of 1000 bars, to 20°C, and to 40°/$_{00}$ salinity. The governing equations for steady flow are:

$$\nabla \cdot \mathbf{v} = 0 \tag{1}$$

$$\mathbf{v} = \frac{K}{\mu}(\rho \mathbf{g} - \nabla p) \tag{2}$$

$$\mathbf{v} \cdot \nabla \mathbf{t} = \frac{k}{(\rho_r c_p)_f} \nabla^2 t \tag{3}$$

$$\rho = \rho_m(s, p)\,[1 - \alpha(s, p)\,|t - t_m(s, p)|^{q(s,p)}] \tag{4}$$

where $\mathbf{v}$ is the Darcy velocity, $\mu$ and $c_p$ are the viscosity and specific heat of the convective fluid and $\rho_r$ is a reference density, which will be $\rho_m$ in equation (4). Also, $K$ and $k$ are, respectively, the permeability and effective thermal conductivity of the saturated porous medium, $p$ and $\mathbf{g}$ are the fluid pressure and gravitational acceleration, $s$ is the salinity level of the water.

It is noted that the first Boussinesq approximation, $\Delta\rho/\rho \ll 1$, is employed in writing the continuity equation (1). The forms and values of the functions $q$, $\alpha$, $\rho_m$ and $t_m$ are given in full detail in ref. [2].

## 2. ANALYSIS

The analysis treats a semi-infinite, horizontal, impermeable surface embedded in a saturated porous medium. No salinity diffusion is considered. The buoyancy arises only due to thermal gradients. The equations for steady, two-dimensional plane flow, with constant properties $\mu$ and $K$, from equations (1)–(3) are then continuity, Darcy's law and energy, as follows:

$$\frac{\partial u}{\partial x} + \frac{\partial v}{\partial y} = 0 \tag{5}$$

$$u = -\frac{K}{\mu}\frac{\partial p_m}{\partial x} \tag{6a}$$

$$v = \frac{K}{\mu}\left[-\frac{\partial p_m}{\partial y} - \frac{\partial p_h}{\partial y} - \rho g\right] \tag{6b}$$

$$u\frac{\partial t}{\partial x} + v\frac{\partial t}{\partial y} = \frac{K}{(\rho_r c_p)_f}\frac{\partial^2 t}{\partial y^2} = \alpha_1 \frac{\partial^2 t}{\partial y^2}. \tag{6c}$$

In Fig. 1, on-flow is on the upper side of the surface for an upward buoyancy force $B$ and on the bottom side for $B$ downwards. In equation (6c) $\alpha_1$ results from the matrix conductivity $k = k_s(1-\varepsilon) + k_f$ where $k_s$, $k_f$ and $\varepsilon$ represent thermal conductivity of solid, fluid and porosity, respectively. This form arose in the evaluation by Katto and Masuoka [17]. The static pressure $p$ is taken as the sum of the local hydrostatic pressure $p_h$ and a motion pressure $p_m$ and $u$ and $v$ are the downstream and normal components of Darcy velocity. Equation (7) below results from an order of magnitude analysis as the boundary-layer approximation.

$$0 = \frac{K}{\mu}\left[-\frac{\partial p_m}{\partial y} + g(\rho_\infty - \rho)\right] \tag{7}$$

The buoyancy force is determined from the density relation, equation (4). In the present analysis, for pure water at 1 bar, $q(0, 1) = 1.894816$

$$\begin{aligned}\rho_\infty - \rho &= \alpha\rho_m(|t - t_m|^q - |t_\infty - t_m|^q)\\ &= \alpha\rho_m|t_0 - t_\infty|^q(|\phi - R|^q - |R|^q)\\ &= \alpha\rho_m|t_0 - t_\infty|^q W\end{aligned} \tag{8}$$

where $t_0$ is the surface temperature, $t_\infty$ is the ambient temperature and $W(x, y)$ is the local buoyancy force. Taking

$$\phi(\eta) = \frac{t - t_\infty}{t_0 - t_\infty} = \frac{t - t_\infty}{d(x)} \tag{9}$$

$$R = \frac{t_m - t_\infty}{t_0 - t_\infty}. \tag{10}$$

A transformation is sought in terms of a similarity variable $\eta(x, y)$. The usual streamfunction $\psi(x, y)$ and $f(\eta)$ are defined following the notation of Gebhart [18]

$$\eta(x, y) = yb(x) \tag{11}$$

$$\phi(x, y) = \alpha_1 c(x) f(\eta) \tag{12}$$

$$p_m = a(x)P(\eta) \tag{13}$$

where $u = \psi_y$, $v = -\psi_x$ and $a$, $b$, $c$ are transformation functions to be determined. The transformation is substituted into (5)–(7) to determine the $a(x)$, $b(x)$, $c(x)$ and $d(x)$, for which similarity will result. The resulting equations in $f$, $\phi$ and $P$ are

$$f' + \frac{K}{\mu}\frac{a\eta b_x}{b^2 c\alpha_1}P' + \frac{K}{\mu}\frac{a_x}{\alpha_1 bc}P = 0 \tag{14}$$

$$P' = \frac{p_m g|t_0 - t_\infty|^q W}{ab} \tag{15}$$

$$\phi'' + \frac{c_x}{b} f\phi' - \frac{cd_x}{bd} f'\phi = 0. \tag{16}$$

For similarity of results, all of the above coefficients

in (14)–(16) must be constants or functions of $\eta$ only. This consideration leads to the following values of $a(x)$, $b(x)$, $c(x)$ and $d(x)$.

$$a(x) = \frac{\mu}{K}\alpha_1 (Ra_x)^{2/3} \tag{17}$$

$$b(x) = Ra_x^{1/3}/x \tag{18}$$

$$c(x) = (Ra_x)^{1/3} \tag{19}$$

$$d(x) = Nx^n \tag{20}$$

where

$$Ra_x = \frac{\alpha K \rho_m g |t_0 - t_\infty|^q x}{\mu\alpha_1} = \frac{\alpha K \rho_m g N^q}{\mu\alpha_1} x^{nq+1}. \tag{21}$$

Note that $Ra_x$ is always positive. In terms of $f$, $P$ and $\phi$ the differential equations and boundary conditions become

$$f' + \frac{nq-2}{3}\eta P' + \frac{2}{3}(\eta q + 1)P = 0 \tag{22}$$

$$P' = W = [|\phi - R|^q - |R|^q] \tag{23}$$

$$\phi'' + \frac{nq+1}{3} f\phi' - nf'\phi = 0 \tag{24}$$

$$f(0) = P(\infty) = \phi(0) - 1 = \phi(\infty) = 0. \tag{25}$$

Note that the above formulation is for flow over the upper side of the surface. For flow on the bottom side of the surface, $P' = -W$. The total buoyancy force out across the boundary region is

$$I_w = \int_0^\infty W \, d\eta = \int_0^\infty [|\phi - R|^q - |R|^q] \, d\eta. \tag{26}$$

This quantity is effective in indicating the net effect of buoyancy in the flow and the flow vigor. In the results in Table 1, $I_w > 0$ is associated with the flow on the upper side of the surface and vice versa. Note that $Pr = \nu/\alpha_1$ does not appear explicitly in the formulation, equation (22), (23) and (24).

Table 1. Calculated values for the isothermal surface condition, $n = 0$, for $q = q(0, 1)$

| $R$ | $f(\infty)$ | $\phi'(0)$ | $P(0)$ | $I_w$ |
|---|---|---|---|---|
| −16 | 7.98224 | −1.22265 | −12.82716 | 12.82716 |
| −8 | 6.50388 | −0.99867 | −8.58169 | 8.58169 |
| −4 | 5.30932 | −0.81915 | −5.80418 | 5.80418 |
| −2 | 4.34997 | −0.67717 | −4.00481 | 4.00481 |
| −1 | 3.58840 | −0.56753 | −2.85906 | 2.85906 |
| −0.5 | 2.99631 | −0.48613 | −2.14937 | 2.14937 |
| 0 | 1.73084 | −0.34181 | −1.21021 | 1.21021 |
| 0.05 | 1.33584 | −0.31326 | −1.08394 | 1.08394 |
| 0.08 | 0.82297 | −0.29031 | −1.00472 | 1.00472 |
| 0.288 | 2.09427 | −0.16919 | 0.10788 | 0.10788 |
| 0.301 | 2.13112 | −0.20009 | −0.02388 | −0.02388 |
| 0.4 | 2.40963 | −0.29639 | −0.51306 | −0.51306 |
| 0.5 | 2.63381 | −0.34915 | −0.83812 | −0.83812 |
| 1 | 3.36983 | −0.48926 | −1.91938 | −1.91938 |
| 2 | 4.21613 | −0.62974 | −3.30297 | −3.30297 |
| 4 | 5.22711 | −0.79009 | −5.27496 | −5.27496 |
| 8 | 6.45335 | −0.98082 | −8.18184 | −8.18184 |
| 16 | 7.95117 | −1.21168 | −12.52490 | −12.52490 |

The role of temperature parameter $R$ is crucial in cold water transport. It expresses the effect of the extremum behavior on the resulting flow. It is an indicator of the relation between $t_0$ and $t_\infty$ and the extremum temperature, $t_m$. It also indicates the nature of the buoyancy force $B$, or $W$. For large $|R|$, the imposed system temperatures are far from the extremum condition. On the other hand, consider $t_0 = 0°C$. Then $R = 1 - t_\infty/t_m$. For $R = 0$, $t_\infty = t_m$ and the buoyancy force is upward over the whole thermal layer, configuration (a) in Fig. 1. However, for $R = 1$, $t_0 = t_m$. The buoyancy force is then downwards, configuration (b). In fact, for $R \leqslant 0$, $W \geqslant 0$ everywhere and the on-flow is on the upper side of a surface. For $R \geqslant 0.5$, $W \leqslant 0$ everywhere and on-flow is on the bottom side of a surface.

In the region $0 < R < 0.5$, $W$ changes sign across the boundary region. As a result, it is not initially known what subrange of $R$ results in a developing boundary-layer flow, either above or below the surface. The computed results, in Table 1, indicate that $I_w > 0$ approaches zero as $R$ increases from $R = 0$. As $R$ decreases from $R = 1/2$, $I_w < 0$ again approaches zero. These are the upper and lower side flows, respectively, in Fig. 1.

## 3. REASONABLE SOLUTIONS

The following basic transport quantities are calculated in terms of similarity variables to determine the imposed temperature conditions, $d(x) = Nx^n$, under which physically realistic solutions result.

$$Q(x) = \int_0^\infty \rho u c_p (t - t_\infty) \, dy \propto cd \times \int_0^\infty f'\phi \, d\eta \propto x^{[n(q+3)+1]/3} \tag{27}$$

$$u(x, y) = \alpha_1 bcf' \propto bc \propto x^{(2nq-1)/3} \tag{28}$$

$$\delta(x) = \frac{\eta}{b} \propto \frac{1}{b} \propto x^{(2-nq)/3} \tag{29}$$

$$\frac{\partial p_m}{\partial x} = -\frac{\mu\alpha_1}{Kx}(Ra_x)^{2/3} \times \left[\frac{2-nq}{3} W\eta + \frac{2}{3}(nq+1)\int_\eta^\infty W \, d\eta\right] \tag{30}$$

$$\dot{m} = \int_0^\infty \rho u \, dy = \alpha_1 \rho c f(\infty) \propto x^{(nq+1)/3} \tag{31}$$

$$M = \int_0^\infty \rho u^2 \, dy = \rho\alpha_1^2 c^2 b \int_0^\infty (f')^2 \, d\eta \propto x^{nq} \tag{32}$$

$$-v(x, y) = \psi_x = \alpha_1 \left[cf'\eta \frac{b_x}{b} + fc_x\right] = \frac{\alpha_1 (Ra_x)^{1/3}}{3x}(f - 2f'\eta) \propto x^{(nq-2)/3}. \tag{33}$$

For a heated or cooled surface, the total local convected energy $|Q(x)|$ should increase or at least remain constant downstream, as for a line source or sink at the leading edge. Thus, from (27), $n \geqslant -1/(q+3)$. From (29), the condition $\delta(0) = 0$ leads to $n \leqslant 2/q$.

Since there is no buoyancy force component in the direction of flow, the flow is completely driven by a pressure field. That is, the favorable pressure gradient in the $x$-direction, $\partial p_m/\partial x < 0$ is the only driving force. Consider equation (30) for $R \leqslant 0$, $W$ and $I_w \geqslant 0$. With the restriction of $-1/(q+3) \leqslant n \leqslant 2/q$, it can be shown that the quantity in the bracket of (30) is positive, and since $Ra_x > 0$. Therefore, $\partial p_m/\partial x < 0$. Thus, on-flow arises above the upper side of the surface. On the other hand, $I_w < 0$ for $R \geqslant 0.5$, and developing flow arises on the bottom side.

## 4. PARTICULAR TRANSPORT CIRCUMSTANCES

There are many important applications to consider. Solutions are given here for only two kinds of temperature conditions. One is an isothermal surface condition in an unstratified ambient medium. Thus $R$ is a constant, $n = 0$, and the equations are

$$f' - \frac{2}{3}\eta P' + \frac{2}{3}P = 0 \tag{34}$$

$$\phi'' + \frac{1}{3}f\phi' = 0 \tag{35}$$

$$P' = [|\phi - R|^q - |R|^q]$$

flow on the upper side of surface (36a)

$$= -[|\phi - R|^q - |R|^q]$$

flow on the bottom side of surface (36b)

$$f(0) = 1 - \phi(0) = \phi(\infty) = P(\infty) = 0. \tag{37}$$

The other condition is that of the bounding surface dissipating a uniform heat flux $q''$. The $Q(x)$ is constant and $n = 2/(q+3)$ from (27). Since $t_0$ varies with $x$, so would $R$ in equation (10), unless $t_\infty = t_m$. Then similarity would be lost in equation (23). Therefore, the condition $R = 0$, or $t_\infty = t_m$ is chosen. The resulting formulation is:

$$(q+3)f' - 2\eta P' + 2(q+1)P = 0 \tag{38}$$

$$(q+3)\phi'' + (q+1)f\phi' - 2f'\phi = 0 \tag{39}$$

$$P' = \phi^q \tag{40}$$

$$f(0) = 1 - \phi(0) = \phi(\infty) = P(\infty) = 0. \tag{41}$$

Some of the particular transport characteristics with an isothermal surface condition are examined next. Both $u$ and $\partial p_m/\partial x$ are seen in equations (28) and (30) to be singular at the leading edge, $x = 0$. The boundary region mass flow, per unit width of surface, $\dot{m}$, is proportional to $x^{1/3}$. The boundary-layer thickness $\delta(x)$ varies as $x^{2/3}$. However, local momentum flux $M$ is independent of $x$. It is recalled that for both vertical and horizontal surfaces embedded in either a Newtonian fluid or porous medium ambient, the normal velocity component $v$ is singular at the leading edge. For example, for a horizontal surface in a Newtonian ambient, $-v = (G/5x)(3f - 2f'\eta)$, the asymptotic solution of $f'$ can be shown to approach zero exponentially at large $\eta$. However, $-v \approx f(\infty)x^{(nq-2)/5}$ Thus, for $n = 0$, $v$ is singular at the leading edge.

Cheng [10] has discarded the possibility of the existence of buoyancy-induced, boundary-layer flow adjacent to an isothermal surface embedded in a porous medium. It was argued that the singularity in the tangential velocity at the leading edge was inadmissably unreasonable. However, the momentum flux $M$ is bounded in (32). Therefore, the singularity of $u(x, y)$ at the leading edge is not obviously worse than that in $v(x, y)$ there.

A consequence of $u(x, y)$ being unbounded at $x = 0$ is that the downstream flow behavior, although quite reasonable, is unusual and very different from most boundary region transport. This is the only configuration in which $u(x, y)$ is unbounded at the leading edge, for both horizontal and vertical surfaces embedded in either a Newtonian fluid or a saturated, porous medium. Finally, the boundary-layer approximation assumes that the gradient in physical quantities are small in the downstream of $x$-direction, when compared with those with $y$. It may be shown that $u/v = O(Ra_x)^{1/3}$. Thus the solutions are more accuracte at increasing $Ra_x$, as is usually found in boundary region flows.

## 5. NUMERICAL RESULTS FOR AN ISOTHERMAL SURFACE CONDITION

Solutions for the isothermal and uniform heat flux surface conditions are presented separately. Isothermal results are considered first. Equations (34)–(36) are a fourth-order system. The accompanying four boundary conditions are designated at two locations, at the surface, $\eta = 0$, and outside the boundary region, $\eta \to \infty$. For computations, $\eta$ must be taken to be finite. Then (34)–(36), with (37), were solved by a predictor–corrector shooting method. The local step size is automatically adjusted to maintain a prescribed accuracy, while integrating from $\eta = 0$ to a chosen $\eta_\infty$. Initial guesses for $\phi'(0)$ and $P(0)$ are successively refined to satisfy the distant boundary conditions. Eventual values of $\phi(\infty)$ and $P(\infty)$ differ from zero by less than $10^{-8}$. In order to ensure convergence of the values of $\phi'(0)$ $f(\infty)$, $P(0)$ and $I_w$ to $10^{-5}$, the value of $\eta_\infty$ was sometimes increased to as much as 55.

Computations were made over a large range of $R$ and into the range of buoyancy force reversal, $0 < R < 1/2$, from both sides, as far as possible. A gap of nonconvergence remained. It was more and more difficult to obtain a convergence further in from each edge $R = 0$ and $1/2$. Flow reversal near the surface first occurred for $R$ decreasing, at around 0.30. The remaining gap was found to be $0.08 < R < 0.288$.

The calculated values of $f(\infty)$, $\phi'(0)$, $P(0)$ and $I_w$, for

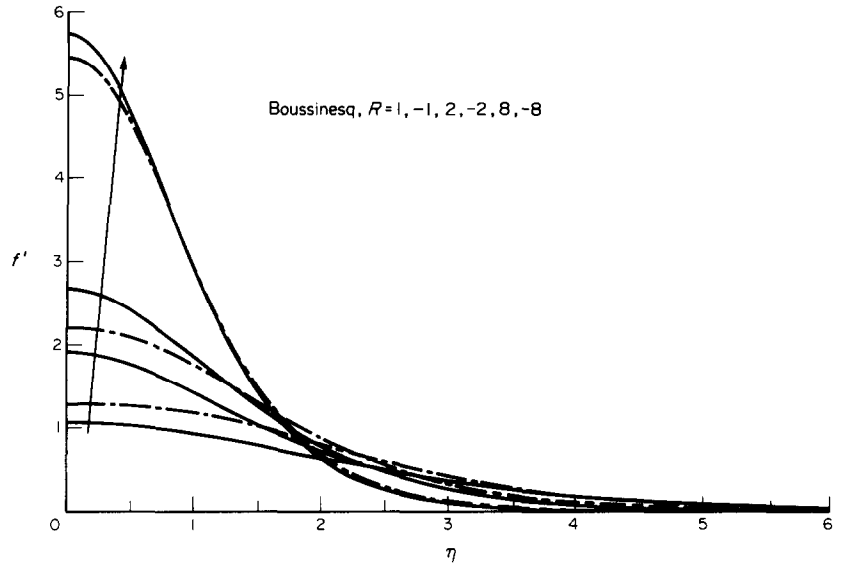


FIG. 2. Distribution of the tangential component of velocity, $f'$, for selected values of $R$ outside the buoyancy reversal region. The solid lines are for flow on the upper side of the surface, the broken lines for flow on the bottom side of the surface.

selected values of $R$, are collected in Table 1. The Boussinesq result, the convectional linear approximation for the density difference in the buoyancy force, is given in Table 3, part A. In Table 1, it is seen that $P(0) = \int_{\infty}^{0} P' \, d\eta = -\int_{0}^{\infty} P' \, d\eta = -I_w > 0$. These flows occur on the upper side of the surface, and extend up into the lower range of local inside buoyancy force reversal, $R \leqslant 0.08$. Similarly, $P(0) = I_w$ for bottom side flows, down into the range of local outside buoyancy force reversal, $R \geqslant 0.288$.

For flow without buoyancy force reversals, calculations were made over a range from $R = -16$ to $+16$, outside the region $0 < R < 1/2$. The Boussinesq buoyancy force approximation is retrieved from the present formulation by choosing $q = 1$. The distributions of the tangential component of the filtration velocity, $f'$, and temperature, $\phi$ for $R = \pm 1, \pm 2, \pm 8$, together with the Boussinesq approximation, as $q = 1$, are shown in Figs. 2 and 3. It appears there that $u_{max}$ for Boussinesq flows is less than that of cold water. It is not, in terms of physical velocity $u = \nu[(Ra_x)^{1/3}/x]f'(\eta)$. Taking specific values, $t_0 = 12.5°C$ and $t_\infty = 12°C$, and

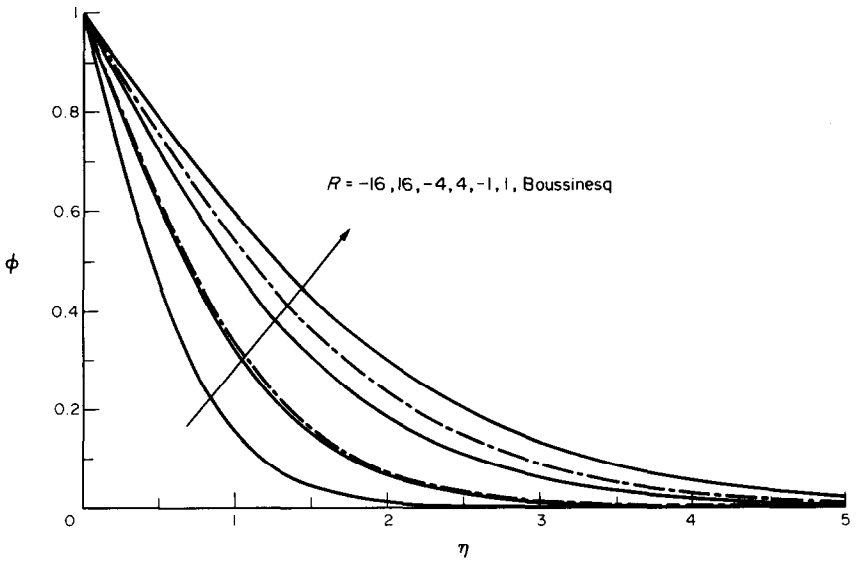


FIG. 3. Distribution of the temperature variation, $\phi(\eta)$, for selected values of $R$ outside the buoyancy reversal region. The solid lines are for flow on the upper side of surface, for $R < 0$, the broken lines for flow on the bottom side of the surface, for $R > 0$.

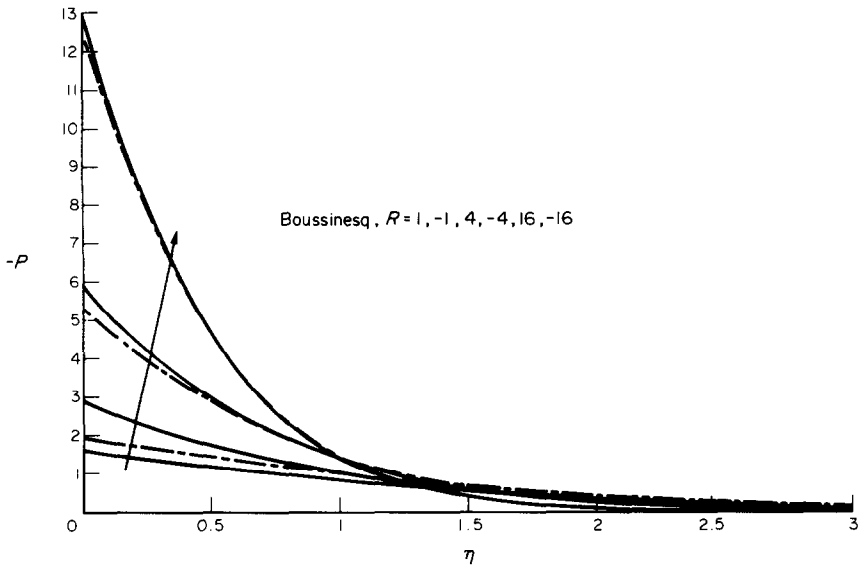


FIG. 4. Motion pressure distribution across the boundary region, for selected values of $R$ outside the buoyancy reversal region. The solid lines are for flow on the upper side of the surface, the broken lines for flow on the bottom side of the surface.

$R = -16$,

$$\frac{u_{max}(\text{cold water})}{u_{max}(\text{Boussinesq})} = \left(\frac{\alpha}{\beta}(t_0 - t_\infty)^{q-1}\right)^{2/3} \frac{f'(0) \text{ cold water}}{f'(0) \text{ Boussinesq}} = 0.977.$$

Figure 4 is the resulting motion pressure distribution for $R = \pm 1, \pm 4, \pm 16$. It is seen that, for increasing $|R|$, the curves for positive and negative values of $R$ merge.

The most surprising result is seen in the variation of the vertical component of velocity component, $v$. Distributions for $R = \pm 1, \pm 2, \pm 4$, together with Boussinesq approximation, are shown in Fig. 5; this component is negative near the surface—i.e. an outflow. Also, there is a $\eta_c$, for each particular value of $R$, at which the slope changes from negative to positive. These distributions are of the same form when plotted against $y$, since $v$ depends linearly on $y$ at any $x$. Recall from (33)

$$\frac{\partial(-v)}{\partial y} = -\frac{\alpha_1 (Ra_x)^{1/3}}{3x} b(x)[f' + 2\eta f''] \qquad (42)$$

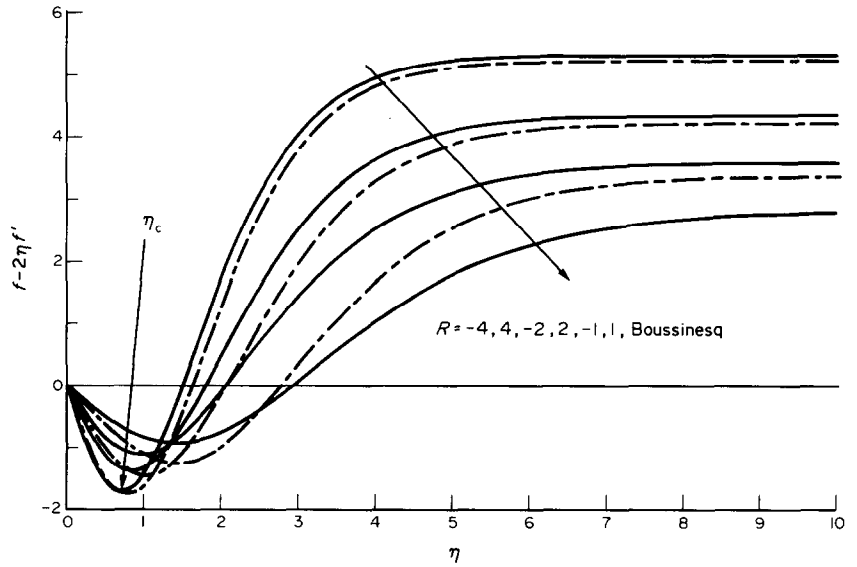


FIG. 5. Distribution of the normal velocity component, $f - 2\eta f'$, for selected values of $R$ outside the buoyancy reversal region. The solid lines are for flow on the upper side of the surface, the broken lines for flow on the bottom side of the surface.

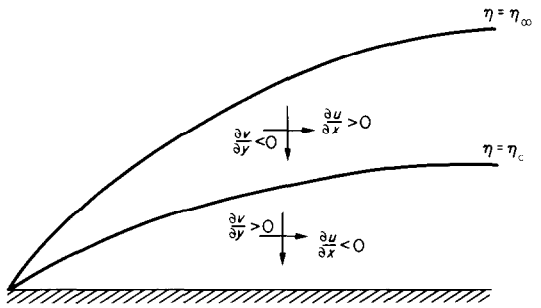


FIG. 6. Boundary-layer buoyancy-induced flow characteristics about a horizontal surface, for $R$ outside of the buoyancy force reversal region.

For any particular value of $Ra$, change in sign of $f' + 2\eta f''$ indicates the intervening extremum in $v$ seen in Fig. 5.

Figure 6 diagrams the general flow characteristics implied by these results, as follows. In the inner region, that is, for $\eta < \eta_c$, $\partial v/\partial y > 0$. Then, from continuity, $\partial u/\partial x < 0$. That is, the tangential velocity component $u$ is decreasing downstream. This generates flow away from the surface. On the other hand, in the outer region flow, for $\eta > \eta_c$, the tangential velocity component is increasing downstream; the normal flow component $v$ then is inward, towards the surface. This is an ordinary entrainment effect.

In fact, this unusual phenomenon, of 'inner region normal velocity component reversal', is common to all buoyancy-induced flows adjacent to horizontal surfaces. However, it was not mentioned in previous studies. It arises both in Newtonian and porous media flow, for both the isothermal and the uniform heat flux boundary conditions. As a specific example, consider a heated surface and the buoyancy force being largest near the surface. This has the tendency to drive the fluid upward. However, any incoming entrainment is a downward flow. Moreover, a favorable motion pressure gradient drives tangential flow downstream. Combining all of these effects, the $v$ velocity distribution will always appear as Fig. 5. Taking specific values for cold water, $t_0 = 6°C$ and $t_\infty = 5°C$, and $R = -1$. Also, for $t_0 = 6°C$ and $t = 5.33°C$, $R = -2$. Since the density of pure water at 1 atm reaches its maximum at 4°C, the buoyancy force $B = g(\rho_\infty - \rho)$, is larger near the surface for $R = -1$ than that of $R = -2$. Therefore, $\eta_c$ would be larger for $R = -1$ than for $R = -2$. This explains the increasing $\eta_c$ in Fig. 5.

Consider next flows with internal buoyancy force reversals, as in the range $0 < R < 1/2$. Calculations were made inward from each of these $R$ boundaries toward any flow reversal or inversion conditions. No convergent solutions were found in the range of $0.08 < R < 0.288$. Again, the transport results for $0 \leqslant R \leqslant 0.08$ and $0.288 \leqslant R \leqslant 0.5$ are in Table 1. It is seen that $P(0) = I_w$ drastically decreases and changes sign near $R = 0.30$, where the gap begins.

However, coming in from the lower side in $R$, $P(0) = I_w$ remains large as the gap is approached. On the other hand, the entrainment velocity parameter $f(\infty)$ decreases substantially across the range $0 \leqslant R \leqslant 0.08$, while over the region $0.288 \leqslant R \leqslant 0.5$, $f(\infty)$ had still retained a comparatively large value. Thus, the characteristics of these two subregions are very different.

Figure 7 shows distributions of the local buoyancy force $W(\eta)$. Though it is not easily inferred in this figure, $W(\eta)$ does change from positive to slightly negative across the thermal region in the range $0 < R \leqslant 0.08$, an outside buoyancy force reversal in upflow. For the other range, $0.288 \leqslant R < 0.5$, $W$ changes sign adjacent to the wall, an inside buoyancy force reversal.

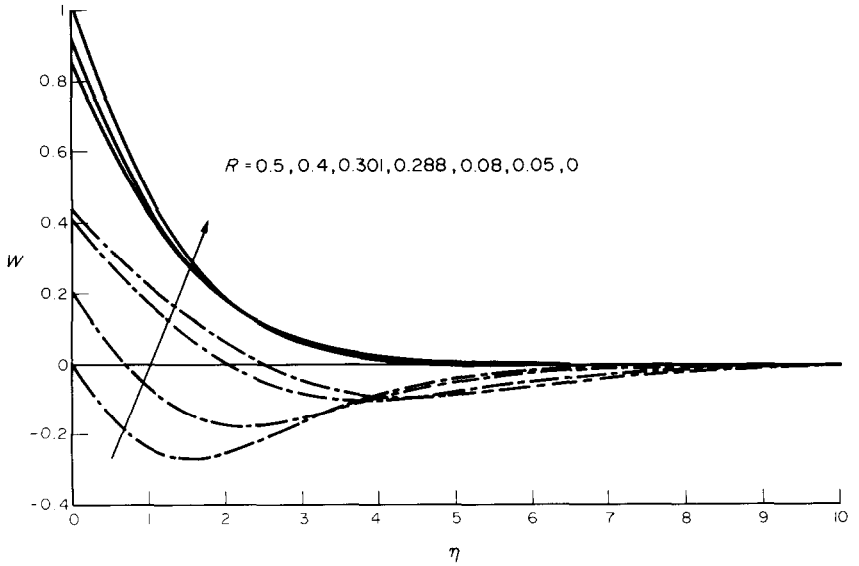


FIG. 7. Distribution of the local buoyancy force, $W$, across the thermal diffusion region. The solid lines are for flow on the upper side of the surface, the broken lines for the flow on the bottom side of the surface.

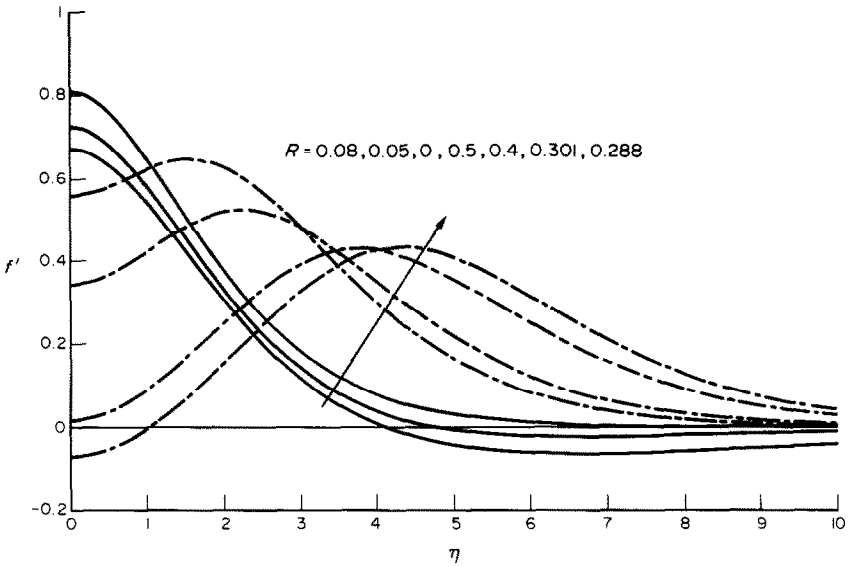


FIG. 8. Distribution of the tangential component of velocity, $f'$, inside the buoyancy reversal region. The solid lines are for the flow on the upper side of the surface, the broken lines for the flow on the bottom side of the surface.

The resulting variations of the tangential component of velocity $u$, for various values of $R$, are plotted in Fig. 8. The calculations detected incipient inside flow reversal as $f'(0)$ first became negative at about $R = 0.30$. Below this value this bidirectional effect increased. On the other hand, very weak outside flow reversal was found over the whole range $0 < R \leqslant 0.08$. Clearly, the boundary region formulation is not reliable for bidirectional flow. The above conditions for incipient flow reversal are indications of the formal limits of such calculations.

The temperature distributions, for selected values of $R$, are shown in Fig. 9. The normal component distributions $v$ are plotted in Fig. 10. It is seen that the behavior with outside flow reversal, that is, for $0 < R \leqslant 0.08$, is now even more complicated than without reversal, in Fig. 5. In the inner part of the layer, a region of normal velocity component reversal again arises, $v$ changes from outward to inward. However, the magnitude of $v$ again decreases at large $\eta$. On the other hand, with inside flow reversal, $v$ again decreases toward the asymptotic value.

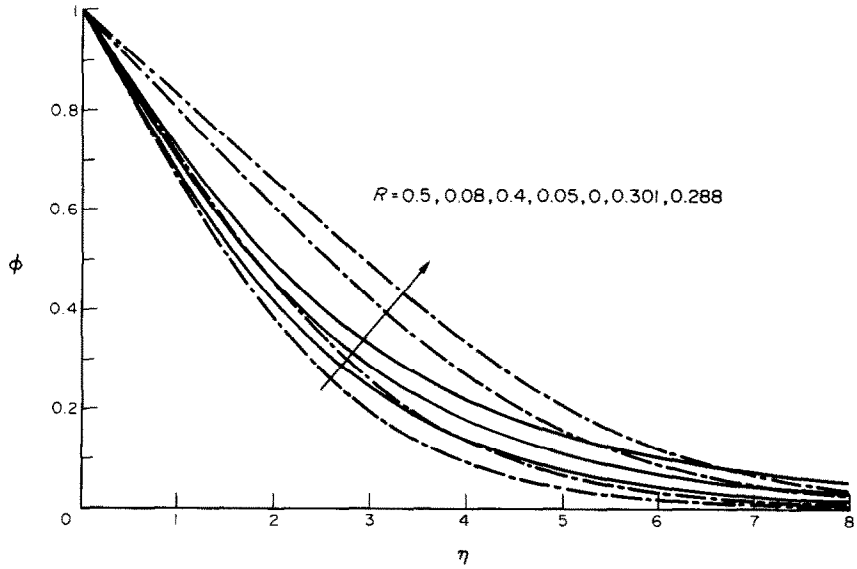


FIG. 9. Distribution of temperature variation, $\phi(\eta)$, inside the buoyancy reversal region. The solid lines are for the flow on the upper side of the surface, the broken lines for the flow on the bottom side of the surface.

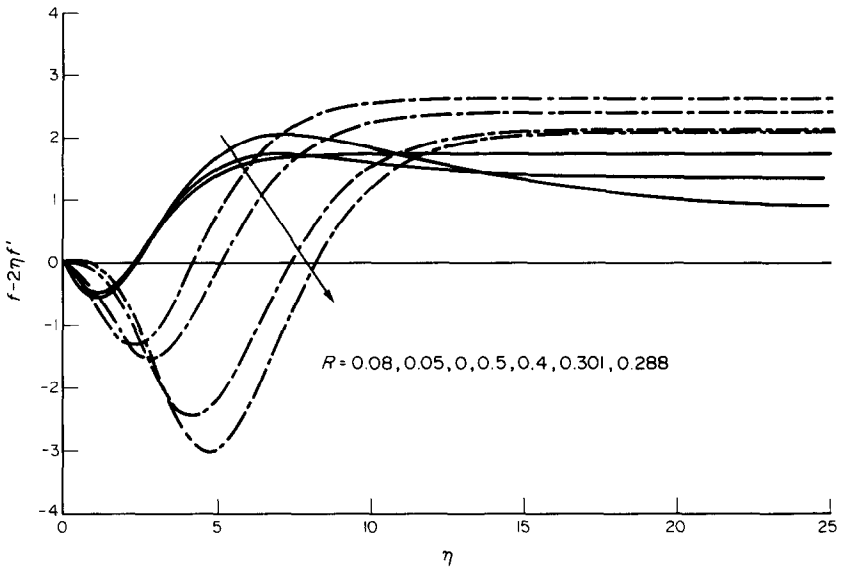


FIG. 10. Distribution of the normal velocity component inside the buoyancy reversal region. The solid lines are for the flow on the upper side of the surface, the broken lines for the flow on the bottom side of the surface.

## 6. A UNIFORM SURFACE HEAT CONDITION

For this imposed condition, equation (27) indicates that the surface temperature increases downstream as $d = t_0 - t_\infty = Nx^n$ where $n = 2/(q+3) = 0.408$, for $q(0, 1)$. For similarity $R$ must be constant downstream. Therefore, in equation (10), since $t_0 = t_\infty = d(x)$, $t_\infty$ must be taken as $t_m$ and $R = 0$. Then $W = W(\eta) \propto (\rho_\infty - \rho)$, the buoyancy force, is always up everywhere across the boundary region, since $\rho < \rho_\infty$. These flows, with upward buoyancy, may be of boundary region form only on the upper side of a surface, for positive heat flux. Again, the resulting transport characteristics, as in equation (26)–(32) for $n = 0$, are calculated for $q = 1.894816$ to be

$$Q(x) \propto x$$

$$u(x, y) \propto x^{(q-1)/(q+3)} = x^{0.183}$$

$$-v(x, y) \propto x^{-2/(q+3)} = x^{-0.408}$$

$$\delta(x) \propto x^{2/(q+3)} = x^{0.408}$$

$$\dot{m} \propto x^{(q+1)/(q+3)} = x^{0.591}$$

$$M(x) \propto x^{2q/(q+3)} = x^{0.774}.$$

Since both $R$ and $Pr$ now no longer appear in the formulation, equations (37)–(40), only one calculation covers all physical circumstances. The resulting entrainment velocity, heat transfer and buoyancy force parameters are collected in Table 2. Conventional results, for $q = 1$ in this formulation, have been calculated by Cheng [10], that is, for $n = 2/(q+3) = 1/2$ and the transport parameters are given in Table 3. The two solutions, for $q = 1.894816$ and for $q = 1$, for the distributions of the tangential velocity component, the temperature and the normal velocity component are plotted in Figs. 11–13, respectively.

In Tables 2 and 3, the Boussinesq result ($q = 1$) has a larger magnitude of $I_w$ than cold water ($q = 1.894816$). Therefore, the velocity level is seen in Fig. 11 to be larger for Boussinesq than that of cold water. Consequently, Boussinesq has a higher heat transfer rate $\phi'(0)$ than cold water as shown in Fig. 12. Again, an inner region of normal velocity component reversal arises, for both the cold water and conventional Boussinesq flows, as shown in Fig. 13.

## 7. CONCLUSIONS

These transport results apply for both isothermal and uniform flux surface conditions for flow adjacent to a horizontal surface submerged in porous medium saturated with cold water. Calculations extend over a wide range of $R$ including conditions both outside and inside the buoyancy force reversal region, $0 < R < 1/2$. Solutions were found outside $0.08 < R < 0.288$.

Outside of $0 < R < 1/2$, it is seen that the velocity, pressure level and heat transfer rate increase as $|R|$ increases. Also for increasing $|R|$, they tend to merge for

Table 2. Uniform flux $n = 2/(q+3) = 0.408593$, $R = 0$, that is $t_\infty = t_m$

| $R$ | $f(\infty)$ | $\phi'(0)$ | $P(0)$ | $I_w$ |
|---|---|---|---|---|
| 0 | 1.07551 | −0.64062 | −0.82141 | 0.82141 |

Table 3. Conventional Boussinesq approximation results

| | | | |
|---|---|---|---|
| (A) Uniform temperature, $n = 0$ | | | |
| 2.81581 | −0.43021 | −1.58362 | 1.58362 |
| (B) Uniform flux, $n = 1/2$ | | | |
| 1.88534 | −0.81646 | −1.14110 | 1.14110 |

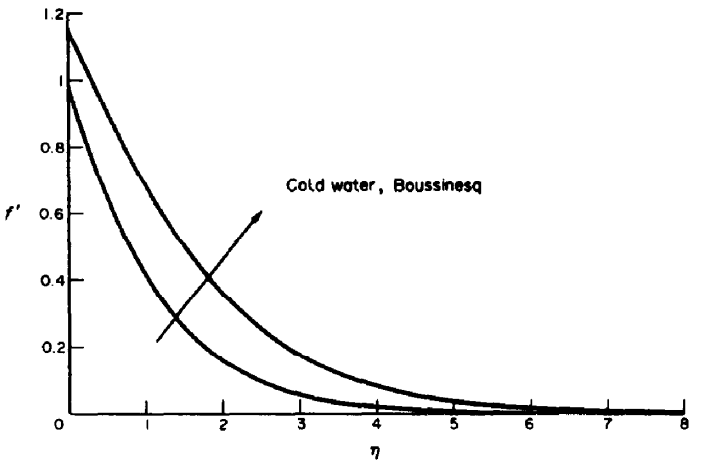


FIG. 11. Distribution of the tangential component of velocity, $f'$, for constant heat flux surface in cold water and conventional Boussinesq approximation.

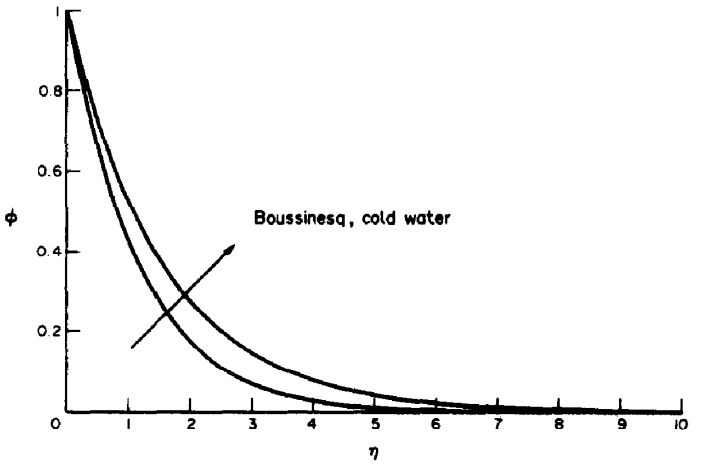


FIG. 12. Distribution of the temperature variation, $\phi(\eta)$, for constant heat flux surface in cold water and conventional Boussinesq approximation.

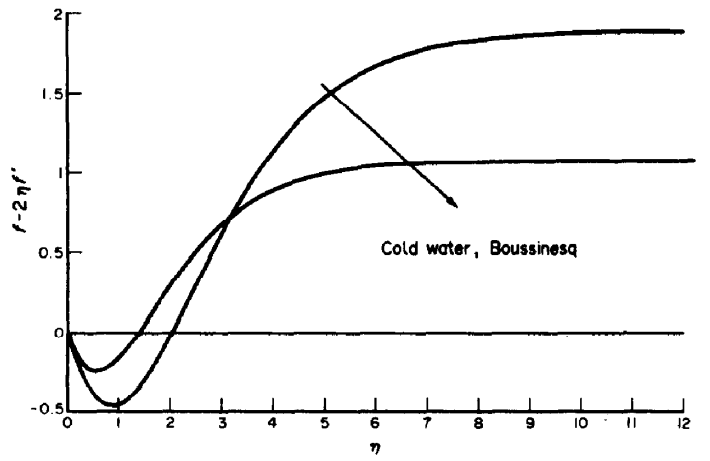


FIG. 13. Distribution of the normal velocity component, $f-2f'\eta$, for constant heat flux surface in cold water and conventional Boussinesq approximation.

positive and negative values of $R$. Moreover, the value of $\eta_c$, at which the slope of the normal velocity component changes from negative to positive, increases as $|R|$ increases.

Dramatic differences in transport arise between conditions of inside and outside buoyancy force reversal. Incipient flow reversal arises inside near the surface at around $R = 0.30$. However, incipient outside local flow reversal occurs over the whole range of $0 < R < 0.08$. The total buoyancy force across the boundary region, $I_w$, decreases substantially as $R$ decreases from 0.5 to 0.288, at the gap. However, $I_w$ remains large as $R$ is increased from 0 to 0.08. The surface heat transfer rate decreases drastically as the nonconvergent gap is approached both from $R = 0$ and $R = 0.5$.

An inner region reversal of normal velocity component was found. Also from Table 1, the lowest surface heat transfer rate is only half of that at both $R = 0$ and $R = 0.5$. No applicable experimental data are available to compare with our results.

*Acknowledgement*—The authors wish to acknowledge support for this study by the National Science Foundation under research grant MEA 82-17756.

## REFERENCES

1. C. T. Chen and F. J. Millero, The specific volume of sea water at high pressures, *Deep Sea Res.* **23,** 595–612 (1976).
2. B. Gebhart and J. C. Mollendorf, A new density relation for pure and saline water, *Deep Sea Res.* **24,** 831–848 (1977).
3. B. Gebhart, M. S. Bendell and H. Shaukatullah, Buoyancy induced flows adjacent to horizontal surfaces in water near its density extremum, *Int. J. Heat Mass Transfer* **22,** 137–149 (1979).
4. Z. H. Qureshi and B. Gebhart, Vertical natural convection with a uniform flux condition in pure and saline water at the density extremum, *Proc. 6th Int. Heat Transfer Conference*, Toronto (1978).
5. V. P. Carey, B. Gebhart and J. C. Mollendorf, Buoyancy force reversals in vertical natural convection flows in cold water, *J. Fluid Mech.* **97,** 279–297 (1980).
6. J. C. Mollendorf, R. S. Johnson and B. Gebhart, Several plume flows in pure and saline water at its density extremum, *J. Fluid Mech.* **113,** 269–282 (1981).
7. B. Gebhart, V. P. Carey and J. C. Mollendorf, Buoyancy induced flows due to energy sources in cold quiescent pure and saline water, *Chem. Engng Commun.* **3,** 555–575 (1979).
8. I. El-Henawy, B. Hassard, B. Gebhart and J. C. Mollendorf, Numerically computed multiple steady states of vertical buoyancy-induced flows in cold pure water, *J. Fluid Mech.* **122,** 235–250 (1982).
9. P. Cheng and W. J. Minkowycz, Free convection about a vertical flat plate embedded in a porous medium with application to heat transfer from a dike, *J. geophys. Res.* **82,** 2040–2044 (1977).
10. P. Cheng and I. D. Chang, Buoyancy induced flows in a saturated porous medium adjacent to impermeable horizontal surfaces, *Int. J. Heat Mass Transfer* **19,** 1267–1272 (1976).
11. P. Cheng, Similarity solutions for mixed convection from horizontal impermeable surfaces in saturated porous media, *Int. J. Heat Mass Transfer* **20,** 893–898 (1977).
12. Z. S. Sun, C. Tien and Y. C. Yen, Onset of convection in a porous medium containing liquid with a density maximum, *Proc. 4th Int. Heat Transfer Conference*, Paris, Versailles, V. IV. NC-211 (1972).
13. Y. C. Yen, Effects of density inversion on free convection heat transfer in porous layer heated from below, *Int. J. Heat Mass Transfer* **17,** 1349–1356 (1974).
14. J. M. Ramilison and B. Gebhart, Buoyancy induced transport in porous media saturated with pure or saline water at low temperatures, *Int. J. Heat Mass Transfer* **23,** 1521–1530 (1980).
15. B. Gebhart, B. Hassard, S. P. Hastings and N. Kazarinoff, Multiple steady state solutions for buoyancy induced transport in porous media saturated with cold pure and saline water, *Numer. Heat Transfer* **6,** 337–352 (1983).
16. L. Pera and B. Gebhart, On the stability of natural convection boundary layer flow over horizontal and slightly inclined surfaces, *Int. J. Heat Mass Transfer* **16,** 1147–1163 (1973).
17. Y. Katto and T. Masuoka, Criterion for the onset of convective flow in a fluid in a porous medium, *Int. J. Heat Mass Transfer* **10,** 297–309 (1967).
18. B. Gebhart, *Heat Transfer*, 2nd edn. McGraw-Hill, New York (1971).

## MOUVEMENT D'ORIGINE THERMIQUE ADJACENT A UNE SURFACE HORIZONTALE SUBMERGEE DANS UN MILIEU POREUX SATURE D'EAU FROIDE

**Résumé**—On présente le calcul de la couche limite laminaire induite par les forces d'Archimède pour un écoulement adjacent à des surfaces horizontales froides ou chaudes immergées dans un milieu poreux saturé d'eau froide avec un éventuel extremum de densité. Les résultats montrent pour la première fois l'existence d'un renversement de composante normale de vitesse. On montre que cela se produit pour tous les écoulements de convection naturelle adjacents à des surfaces horizontales. On note que le nombre de Prandtl $Pr = \nu/\alpha_l$ n'apparait pas comme un paramètre additionnel dans cette formulation. Un paramètre de température $R$ exprime la relation entre les températures imposées $t_0$ et $t_\infty$ et la température $t_m$ de l'extremum. Des calculs sont conduits à la fois pour des conditions de renversement. Pour une surface isotherme, les résultats pour $0 \leqslant R \leqslant 0{,}08$ et $0{,}288 \leqslant 5 \leqslant 0{,}5$ incluent les régions de renversement. Les caractéristiques de ces deux sous-régions sont différentes. Des tabulations détaillées des paramètres de transport sont données pour les deux types de conditions aux limites. Ces nouveaux résultats sont comparés avec ceux résultants de l'approximation conventionnelle de Boussinesq.

## AUFTRIEBSINDUZIERTE STRÖMUNG ENTLANG EINER HORIZONTALEN OBERFLÄCHE IN EINEM PORÖSEN, MIT KALTEM WASSER GESÄTTIGTEN MEDIUM

**Zusammenfassung**—Es werden Transportberechnungen für die laminare Grenzschicht einer auftriebsinduzierten Strömung entlang beheizter oder gekühlter horizontaler Oberflächen durchgeführt. Die Oberflächen befinden sich in einem porösen Medium, das mit kaltem Wasser gesättigt ist, wobei ein Dichteextremum auftreten kann. Die Ergebnisse zeigen zum ersten Mal die Existenz eines inneren Gebietes mit Umkehr der senkrechten Geschwindigkeitskomponente. Es zeigt sich, daß dies für alle natürlichen Konvektionsströmungen entlang horizontaler Oberflächen auftritt. Bemerkenswert ist, daß die Prandtl-Zahl $Pr = \nu/a_l$ nicht als zusätzlicher Parameter in dieser Beschreibung erscheint. Ein Temperaturparameter $R$ beschreibt den Zusammenhang zwischen den aufgeprägten Temperaturen $t_0$ und $t_\infty$ und der Extremtemperatur $t_m$. Es werden Rechnungen für eine isotherme Oberfläche und für eine konstante Wärmestromdichte über einen weiten Bereich von $R$ durchgeführt, die Umkehrbedingungen für die Auftriebskraft enthalten. Bei der isothermen Oberfläche ergeben sich Gebiete der Umkehr der Auftriebskraft für $0 \leqslant R \leqslant 0{,}08$ und $0{,}288 \leqslant R \leqslant 0{,}5$. Die Eigenschaften dieser beiden Unterregionen sind verschieden. Genaue Tabellen der Transportparameter sind sowohl für die isotherme Oberfläche als auch für konstante Wärmestromdichte enthalten. Diese Ergebnisse werden mit denen nach der konventionellen Boussinesq-Approximation verglichen.

## ТЕЧЕНИЕ, ВЫЗВАННОЕ ПОДЪЕМНОЙ СИЛОЙ, ВОЗНИКАЮЩЕЕ У ГОРИЗОНТАЛЬНОЙ ПОВЕРХНОСТИ, НАХОДЯЩЕЙСЯ В ПОРИСТОЙ СРЕДЕ, НАСЫЩЕННОЙ ХОЛОДНОЙ ВОДОЙ

**Аннотация**—Представлены расчеты процессов переноса для ламинарного пограничного течения, вызванного подъемной силой, около нагретой или охлажденной горизонтальной поверхности, помещенной в насыщенную холодной водой пористую среду, в которой может возникнуть экстремальное значение плотности. С помощью полученных результатов впервые показано существование "внутренней зоны обращения направления нормальной компоненты скорости". Отмечено также, что это является общим свойством всех естественноконвективных течений у горизонтальных поверхностей. Показано, что в данной постановке число Прандтля $Pr = \nu/\alpha_1$ не появляется в качестве дополнительного параметра. Температурный параметр $R$ выражает связь заданных температур $t_0$ и $t_\infty$ с экстремальным значением температуры $t_m$. Проведены расчеты для изотермических условий и однородного потока на поверхности в широком диапазоне изменения $R$, включая условия обращения подъемной силы. Для изотермической поверхности результаты переноса при $0 \leq R \leq 0{,}08$ и $0{,}288 \leq R \leq 0{,}5$ учитывают области обращения подъемной силы. Обнаружено несовпадение характеристик этих двух областей. Составлены подробные таблицы параметров переноса как для изотермической поверхности, так и для однородного потока. Найденные результаты сравниваются с результатами, полученными в приближении Буссинеска.